(NASA-CR-131841) ELECTROSTATIC PROPULSION BEAM DIVERGENCE EFFECTS ON SPACECRAFT SURFACES. VOLUME 2, ADDENDUM 1: ION TIME-OF-FLIGHT DETERMINATIONS OF (TRW Systems Group) 48 p HC $4.50 CSCL 21C G3/28

N73-26795

Unclas 06663

# ELECTROSTATIC PROPULSION BEAM DIVERGENCE EFFECTS ON SPACECRAFT SURFACES

## VOLUME II
## FINAL REPORT
## ADDENDUM NO. 1

ION TIME-OF-FLIGHT DETERMINATIONS OF DOUBLY TO SINGLY IONIZED MERCURY ION RATIOS FROM A MERCURY ELECTRON BOMBARDMENT DISCHARGE

**TRW NO. 11985-6002-RU-01** -VOL-2-ADD

**J. M. SELLEN, JR., R. F. KEMP, AND DAVID F. HALL**

**19 APRIL 1973**

**CONTRACT NO. 952350**

This work was performed for the Jet Propulsion Laboratory, California Institute of Technology, sponsored by the National Aeronautics and Space Administration under Contract NAS7-100.

**Prepared for**

**JET PROPULSION LABORATORY**
**CALIFORNIA INSTITUTE OF TECHNOLOGY**
**PASADENA, CALIFORNIA**

TRW
SYSTEMS GROUP

CONTENTS

## ILLUSTRATIONS

# ION TIME-OF-FLIGHT DETERMINATIONS OF DOUBLY TO SINGLY IONIZED MERCURY ION RATIOS FROM A MERCURY ELECTRON BOMBARDMENT DISCHARGE

J. M. Sellen, Jr., R. F. Kemp, and David F. Hall
TRW Systems Group
Redondo Beach, California

## I. INTRODUCTION

The efficient operation of mercury electron bombardment ion thrusters for spacecraft propulsion requires a maximization of propellant utilization (i.e., the conversion of neutral mercury vapor to mercury ions) and an acceleration of the mercury ions to the optimum specific impulse for a given mission profile. Both of these goals may be adversely affected by the presence of multiply charged mercury ions in the thruster exhaust beam. For charge states higher than singly ionized mercury, the larger value of q/m for the particle (where q and m are particle charge and mass) leads to exhaust velocities which exceed the optimum specific impulse (assuming here that singly ionized mercury ions are accelerated to the optimum velocity) with a consequent loss of thrust efficiency. The presence of multiply charged ions in the exhaust beam also complicates the determination of propellant utilization when that utilization is based upon total exhaust ion current divided by the current equivalent of the injected neutral mercury vapor flow. Failure to correct the ion exhaust beam current flow for multiply charged ion species will lead to errors in the specification of propellant utilization for the thruster, with subsequent adverse effects on spacecraft mission performance. This program was undertaken to obtain data useful in establishing performance and test criteria for ion thrusters and in mission design. The resultant data have also provided a new approach to the diagnosis of electron bombardment discharge processes.

The first experiments to determine the abundance of multiply charged ions in a thruster exhaust were conducted in 1962 by Milder[1] and by Kemp, Sellen, and Pawlik.[2] Using a magnetic analyzer and hot wire current detecting probes, Milder obtained $Hg^{++}/Hg^{+}$ ratios (hereafter denoted as ++/+ ratios) as a function of the anode potential in the electron bombardment discharge. The onset of doubly charged ions was observed as

discharge potential was increased above ∿20 volts, and ++/+ ratios as large as 0.2 were obtained for anode potentials of 100 volts. The abundance of $Hg^{++}$ relative to $Hg^{+}$ for these experiments appeared to be larger than would occur if only single stage processes occurred (i.e., the production of $Hg^{+}$ and $Hg^{++}$ by a single ionizing collision of an electron) and suggested that "sequential processes" were at work (i.e., the production of $Hg^{++}$ by successive ionization encounters each of which resulted in the removal of a single electron). Milder also searched for $Hg^{+++}$, but was not able to detect this species, noting, however, that resolution of the magnetic analyzer was such that small quantities of the triply charged ion could be present without system detection.

Kemp, Sellen, and Pawlik in their early experiments detected $Hg^{++}$ by two methods. The first method utilized a pulsed ion engine acceleration voltage with the ion current to a distant collector recording the arrival of, at first, the more rapidly moving doubly charged ions, and, after an appropriate delay, the arrival of the more slowly moving $Hg^{+}$ ions. The ++/+ ratio was approximately 0.06 which, for the discharge potential of 50 volts, was in comparatively good agreement with the results of Milder. The second experimental treatment of the ++/+ ratio utilized a steady-state ion exhaust beam flow into an ion velocity analyzer (operating as a shortened Wien velocity filter). Abundance ratios from this analyzer were in agreement with those obtained by the pulsed beam ion time-of-flight technique. When the discharge potential was increased to 100 volts, the pulsed beam tests revealed the presence of $Hg^{+++}$.

More recently, Masek[3] performed exploratory measurements on a mercury ion engine exhaust with a variable field magnetic analyzer. Doubly charged ions of mercury were observed, but system resolution was not sufficient for other than order of magnitude measurements. The improvement of resolution in this experiment has led to the current findings by Pawlik, Goldstein, Fitzgerald, and Adams.[4] Their measurements (as had those of Milder) revealed an onset in $Hg^{++}$ production for anode discharge potentials in excess of ∿23 volts, and were interpreted as suggesting that $Hg^{++}$ is not produced, in the main, by single stage ionization processes from the $Hg^{0}$ ground state. Their experiments also revealed significant variations in the ++/+ ratio as a function of position over

the face of the accelerator grid of the ion engine with predominant ++ production on the axis of the thruster and reduced ++ production near the boundaries of the engine. These measurements were also interpreted as evidence that sequential ionization to the doubly ionized state is the principal means for the production of this ion species.

The experiments and analysis to be reported here will both continue and extend the previous investigations. The ion engine in use in the experiments is a 20-cm-diameter electromagnet electron bombardment ion engine and is similar to that utilized by Pawlik et al.[4] The experimental technique to determine ++/+ abundance ratios utilized ion time-of-flight, but was a variation of that technique used in the earlier tests of Kemp, Sellen, and Pawlik.[2] There, the entire ion beam was pulsed on rapidly. In the present experiments, the ion flow from the ion engine is constant. A section of that ion flow enters an analyzer and is acted upon there by a transverse electric field which bends the ions. The rapid release of this deflection field allows the undisturbed ion flow to proceed directly into a Faraday cup with ion time-of-flight now occurring within the confines of the analyzer. This technique will be discussed further. In addition, an analytical treatment of the discharge action in producing various ion species has been carried out. That analysis is presented in the following section, and will be followed by a description of the time-of-flight technique, experimental results, and a discussion of those results.

## II. ANALYSIS OF DISCHARGE PROCESSES

In his treatment of $Hg^+$ and $Hg^{++}$ from electron bombardment discharges, Milder[1] identified three reactions as the basis of a simple analysis. Pawlik et al[4] broadened the number of reactive processes to be considered to include ionization of both atoms and ions from states other than the ground state. In a more recent work, Wu[5] has numerically evaluated reaction rates for a series of possible ionization processes. In these calculations, it has been assumed that electrons possess a Maxwellian energy distribution.

The following analysis differs somewhat in concept from previous approaches. Its basis is a consideration of a group of neutral mercury atoms, of number $n_o$, as that group moves through the electron bombardment discharge. In an actual ion engine, neutrals moving through the discharge undergo various changes of state in both ionization and excitation. The particles so formed may move to the exit plane of the engine, pass through the openings in the screen grid and undergo acceleration. They may also intercept warm material surfaces within the discharge chamber. It is assumed that interception with such surfaces returns the mercury particle to the ground state of the neutral atom, whereupon it re-evaporates and re-enters the discharge. At some point in the particle "history" in the discharge, the particle trajectory will result in passage through the accelerator grid. The analysis will focus attention on that portion of the particle path between its last interception with a material surface and its passage through the accelerator grid. This geometry is shown in Figure 1.

Considering a group of $n_o$ atoms and denoting $t = 0$ as the instant of the last contact with a material boundary before passage through the accelerator, the following equations may be written:

$$\frac{dn_o}{dt} = - F_{01} n_e n_o - F_{02} n_e n_o \qquad (1)$$

$$\frac{dn_+}{dt} = F_{01} n_e n_o - F_{12} n_e n_+ \qquad (2)$$

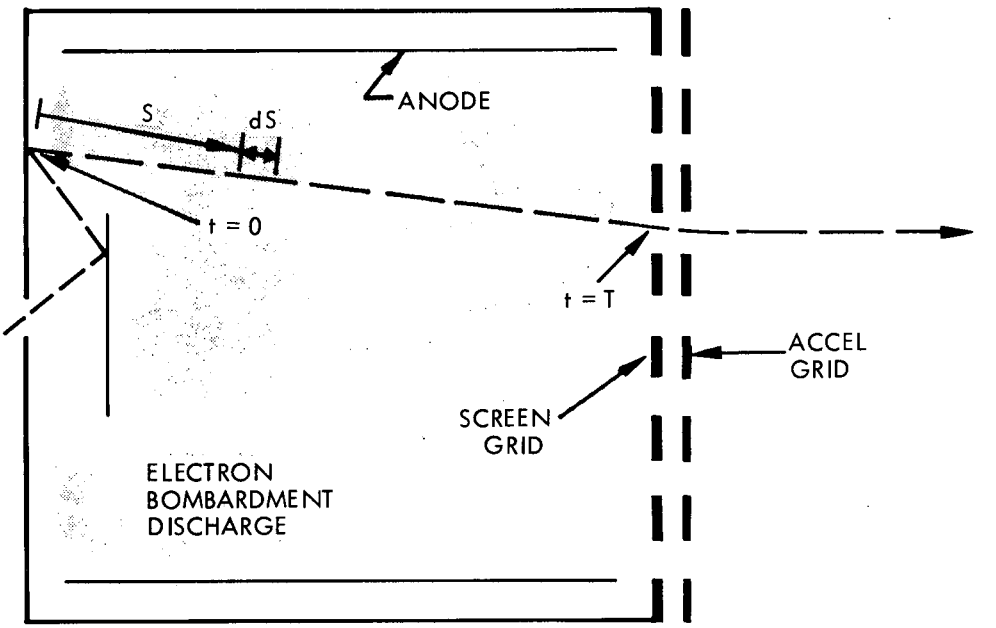


Figure 1. Simplified Discharge Configuration Considered in the Analysis. At t = 0 the neutral mercury atom completes its final encounter with a material boundary before passage through the accelerator grid at t = T. Excitation and ionization of the particle occurs along the trajectory, resulting in various abundance levels of $Hg^0$, $Hg^+$, and $Hg^{++}$.

$$\frac{dn_{++}}{dt} = F_{02} n_e n_o + F_{12} n_e n_+ \tag{3}$$

The quantities $n_e$, $F_{01}$, $F_{02}$, and $F_{12}$ are defined below. Equations (1), (2), and (3) have considered three possible reactive processes:

$$e + Hg^0 \longrightarrow Hg^+ + e + e \tag{4}$$

$$e + Hg^0 \longrightarrow Hg^{++} + e + e + e \tag{5}$$

and

$$e + Hg^+ \longrightarrow Hg^{++} + e + e \tag{6}$$

In the description here no assumption will be made concerning the excitation states of $Hg^0$, $Hg^+$, or $Hg^{++}$. Thus, metastable levels of $Hg^0$ are included in the process given by Equations (4) and (5). Similarly, the ions on the left hand side in Equation (6) may be in either the ground state or excited states.

In writing Equations (1), (2), (3) as the sole reactive processes for treatment, the analysis has not considered electron-ion recombination reactions or charge exchange processes (while charge exchange between $Hg^0$ and $Hg^+$ does not result in a change in specie abundance, charge exchange between $Hg^{++}$ and $Hg^0$ which leads to 2 $Hg^+$ would alter such abundances). Also neglected here are the third and higher steps in the sequential ionization chain. The term $n_e$ is electron density ($cm^{-3}$) and it is important to note that, in an actual discharge, major changes will occur in this variable as particles move along their paths (increasing t). In addition to changes in the magnitude of $n_e$, the energy distribution of electrons also changes from point to point in the discharge. The energy distribution function for electrons will be denoted as $f_e$ where

$$\int_0^\infty f_e(E)\, dE = 1 \tag{7}$$

The final terms to be defined are $F_{01}$, $F_{02}$, and $F_{12}$. In general,

$$F_{ij} = \int_0^\infty f_e(E)\, v_e\, \bar{\sigma}_{ij}(E)\, dE \tag{8}$$

is a net transfer probability (in $cm^3/sec$) from the $i^{th}$ to the $j^{th}$ state of ionization. When multiplied by $n_e$ (electrons/$cm^3$) $n_e F_{ij}$ has the dimensions of $t^{-1}$. Note that the definition of $F_{ij}$ utilizes $\bar{\sigma}_{ij}$ as a cross section for the transition from the $i^{th}$ to the $j^{th}$ ionization state. To make Equation (8) completely general $\bar{\sigma}_{ij}$ includes transitions from all possible excitation levels in the $i^{th}$ state (thus $\bar{\sigma}_{01}$ includes ionization from metastable neutral states). The use of the $\bar{\sigma}_{ij}$ notation is meant to indicate an appropriate weighting of the cross sections to be utilized over the distributions of $n_0$ and $n_+$ in their initial states of the reaction.

Returning to Equations (1), (2), and (3) and with the specification of Equation (8), it is possible in principle, to evaluate specie abundance from the original group of $n_0$ atoms through integration along the particle path through the discharge (note that an integral in t may be transformed into an integral in s, distance along the particle trajectory, through use

of the relation ds = $v_p$ dt). Finally, to evaluate the total ++/+ ratio in the emerging ion beam, a weighted average would be required for each exit hole in the accelerator grid, with appropriate weight to all of the possible particle trajectories which ended in passage through the hole, followed by a summation, with appropriate weighting in current/hole, over the totality of holes in the exit grid.

While the procedure outlined would result in an evaluated ++/+ ratio for the exhaust beam, the estimated extent of required numerical calculations are considerable and beyond the intent of the present analysis. Variations in $f_e$ and $n_e$ occur along the particle path, and considerable uncertainty exists over certain elements of the terms in $\bar{\sigma}_{ij}$. From the measurements of Masek,[6] electrons in the discharge consist of both "high energy primary" electrons and a Maxwellian group of "secondary electrons" with radically differing ionization probabilities because of the strong energy dependence in those terms. Moreover, from the recent measurements of Wilbur,[7] plasma potential variations in the discharge regions are of a complicated nature with accompanying complications in electron density and temperature. The potential variations in the plasma discharge impact upon integrals in time along the particle paths because of velocity changes of charged particles in the discharge electric fields (dt and ds are linked by $v_p$, particle velocity). Of even further concern but not, as yet, treated, are particle orbit changes due to the turbulence of the electric fields in the plasma discharge.

In view of the many real difficulties in assessing the ++/+ ratio by a rigorous evaluation of Equations (1 through 3) with appropriate weighting, an analytical approach would appear to be unwarranted. However, some qualitative insight into discharge behavior might be gained by a simple integration of these equations. The results could then be compared to the results of experiments to note if discharge behavior can be predicted on, at least, a parametric basis. When these integrations are carried out the results are:

$$n_o(T) = n_o(0)e^{-n_e(F_{01} + F_{02})T} \tag{9}$$

$$n_+(T) = \frac{n_o(0)F_{01}}{F_{12} - (F_{01} + F_{02})} \left\{ e^{-n_e(F_{01} + F_{02})T} - e^{-n_e F_{12} T} \right\} \tag{10}$$

$$n_{++}(T) = \frac{n_o(0)F_{02}}{F_{01} + F_{02}} \left(1 - e^{-n_e(F_{01} + F_{02})T}\right) + \frac{n_o(0)F_{01}F_{12}}{F_{12} - (F_{01} + F_{02})} \left[ \frac{\left(1 - e^{-n_e(F_{01} + F_{02})T}\right)}{F_{01} + F_{02}} - \frac{\left(1 - e^{-n_e F_{12} T}\right)}{F_{12}} \right] \tag{11}$$

These straightforward results are, of course, only obtained in the case where $n_e$ and $F_{ij}$ are invariant along the path of integration. With this as the principal simplifying assumption, estimates of the ++/+ ratio can be obtained for comparison to experimental findings.

Note that the abundances are given in terms of the particle time of flight, T, from the last encounter with a material boundary and until passage through the acceleration grid. For the exhaust beam of an ion engine, the value of T will be given approximately by $L/v_p$ where L is the final drift path length in the discharge region and $v_p$ is particle drift speed averaged over the passage through the discharge. Considering a drift distance of $\sim$10 cm, a particle having 0.05 ev ($\sim$500°K) thermal energy would travel at $\sim 10^4$ cm/sec and escape through the accelerator grid in $10^{-4} < T < 10^{-3}$ sec. To evaluate the ++/+ ratio, Equation (11) is divided by Equation (10) to yield

$$\frac{n_{++}}{n_+} = \frac{\left[ \frac{F_{12}}{F_{01}+F_{12}} \left(1 - e^{-n_e(F_{01}+F_{02})T}\right) - \left(1 - e^{-n_e F_{12} T}\right) + \frac{F_{02}}{F_{01}} \left( \frac{F_{12} - (F_{01}+F_{02})}{(F_{01}+F_{02})} \right) \left(1 - e^{-n_e(F_{01}+F_{02})T}\right) \right]}{\left[ e^{-n_e(F_{01} + F_{02})T} - e^{-n_e F_{12} T} \right]} \tag{12}$$

Equation (12) is not easily visualized in general in terms of ion abundance. However, some simplification may be made in the context of conventional ion engine operating conditions. Ion engines, if they are

to be utilized as thrusting devices, must have a high propellant utilization efficiency. Since the emerging neutral fraction of the initial neutral input is given by $e^{-n_e(F_{01} + F_{02})T}$, a high propellant utilization requires that the discharge conditions be such as to yield $|n_e(F_{01} + F_{02})T|$ of at least 2.

An alternative statement of this condition is that the discharge must be "thick" to the removal of mercury from its neutral state. A second implied condition in efficient ion engine operation is that the discharge must be "thin" with regard to delivery of the particles into the doubly ionized state. These conditions are, in fact, obtained in the present development of ion engines, and, with these known indications on the magnitude of particular ionization levels, Equation (12) may be simplified to

$$++/+ = \frac{n_e F_{12} T - \varepsilon \eta - \beta \eta(\varepsilon - 1)}{\eta - n_e F_{12} T} \tag{13}$$

where $\eta$ is the fractional propellant utilization efficiency $(\frac{n_o(0) - n_o(T)}{n_o(0)})$, $\varepsilon = \frac{F_{12}}{F_{01} + F_{02}}$ and $\beta = \frac{F_{02}}{F_{01}}$. In the limit of propellant utilization near unity this expression becomes

$$++/+ = \frac{n_e F_{12} T - \varepsilon + \beta - \varepsilon\beta}{1 - n_e F_{12} T} \tag{14}$$

This is the expression which shall be used in an examination of experimental results. It should be noted that both $\beta$ and $\varepsilon$ are energy dependent terms. Increases in anode discharge potential will presumably lead to a more energetic electron distribution for which both $F_{02}$ and $F_{12}$ will increase relative to $F_{01}$ thus increasing both $\varepsilon$ and $\beta$. It should also be noted that the only plasma density dependent term in the ++/+ ratio appears in $n_e F_{12} T$. Thus, variations in the discharge which result in increases in plasma density and which do not result in alterations in the electron energy distribution should affect the ++/+ ratio through

the $n_e F_{12} T$ term, and experiments revealing such density dependent behavior would be evidence that sequential ionization does occur in the discharge (non-zero $F_{12}$).

It is also of interest to examine Equation (14) in the limit that certain transitional probabilities vanish. For example, if $F_{12}$ is set equal to zero, then doubly charged ions appear only through the $0 \rightarrow 2$ transition. Examining (14) in this limit

$$++/+ = \beta\big|_{\lim F_{12} \to 0} = \frac{F_{02}}{F_{01}} \tag{15}$$

This, it may be noted recovers the situation originally treated by Milder [Equation (9), Reference 1].

To illustrate the agreement between exact and approximate forms of the ++/+ ratio, Equation (12) has been evaluated as a function of $n_e/\hat{n}_e$, electron density normalized to the value for which $\hat{n}_e F_{01} T = 2$, $F_{02} = 0.01\ F_{01}$ and $F_{12} = 0.1\ F_{01}$. These calculations are illustrated in Figure 2. As $n_e/\hat{n}_e \rightarrow 0$, the ++/+ ratio goes to $0.01 = F_{02}/F_{01}$. Thus $++/+ \rightarrow F_{02}/F_{01}$ as $n_e \rightarrow 0$, irrespective of the magnitude of $F_{12}$, and, also from Equation (15), as $F_{12} \rightarrow 0$, irrespective of the magnitude of $n_e$. Note that Equation (13) cannot be used for expressions of ++/+ in the limit of $n_e \rightarrow 0$, since this approximate form of Equation (12) has a required condition of high propellant utilization which fails in the limit of vanishing electron density. For conditions in which propellant utilization is high, Equation (14) is in good agreement with the exact expression [Equation (12)] as may be noted in the curves of Figure 2.

Another condition to examine is the limit of Equation (14) in the limit $F_{02} \rightarrow 0$. This condition is a comparatively likely one for discharge anode potentials less than ~35 volts. Setting $F_{02}$ to zero yields

$$\left.\frac{++}{+}\right|_{\substack{\lim \\ F_{02} \to 0}} = \frac{n_e F_{12} T - \varepsilon}{1 - n_e F_{12} T} \tag{16}$$

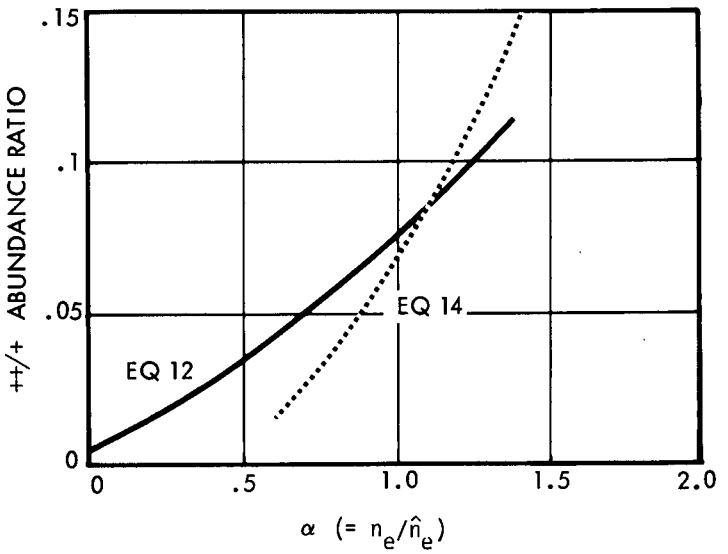


Figure 2. The ++/+ Abundance Ratio versus Normalized Electron Density. Normalization is to $\hat{n}_e$, that density for which $\hat{n}_e F_{01} T = 2$. $F_{12}/F_{01} = 0.1$, and $F_{02}/F_{01} = 0.01$.

where $\epsilon = \dfrac{F_{12}}{F_{01} + F_{02}}$ now becomes $\dfrac{F_{12}}{F_{01}}$.

For $n_e F_{12} T \ll 1$, (a discharge "thin" with respect to the second step in the sequential ionization), then (16) may be approximated by

$$++/+ \doteq n_e F_{12} T (1 + n_e F_{12} T)\left(1 - \frac{1}{n_e F_{01} T}\right) \tag{17}$$

Since the discharge in the engine is "thick" for the first ionization for cases of practical interest, the term $n_e F_{01} T$ is "large" and is essentially invariant for changes in, for example, discharge anode potential.

Equation (17) may then be further approximated to

$$++/+ \doteq n_e F_{12} T (1 + n_e F_{12} T) \tag{18}$$

and

$$\frac{\partial(++/+)}{\partial V_{anode}} \doteq \frac{\partial(n_e F_{12} T)}{\partial V_{anode}} (1 + 2\, n_e F_{12} T) \tag{19}$$

Thus, if the anode potential can be varied without variations being introduced in plasma density, then electron energy distributions will be altered, and $F_{12}$ will be altered. Since $F_{12}$ rises with increasing electron energy, $\partial F_{12}/\partial v_{anode}$ should be expected to be > 0 and $\frac{\partial(++/+)}{\partial v_{anode}}$ is expected to be positive.

In conclusion to this present discussion, it should be emphasized again that the purpose of the analysis is to gain insight into ion engine behavior in at least its parametric dependences. It is recognized that the ion engine and its discharge is, in the overall sense, a complicated process. Analyses of ion engine propellant utilization, such as those by Kaufman[8] and Kaufman and Cohen[9] indicate that neutral propellant losses at high discharge loss conditions are approximately constant, irrespective of the total neutral injection flow rate. From this evidence, there are processes present in the engine discharge which are not represented in the original discharge Equations (1), (2), and (3), or if present, are subject to subtle changes as the neutral injection rate is varied. The analysis in this present treatment, then, operates with clearly acknowledged limitations, but with the possibility of some practical application.

## III. ION TIME-OF-FLIGHT (TOF) TECHNIQUE

### A. OPERATIONAL PRINCIPLES AND PROBLEMS IN ION TOF ANALYZERS

The principles of ion time-of-flight as a means of identifying ion charge species in the exhaust beam of an ion engine, were first used by Kemp, Sellen, and Pawlik.[2] In those experiments the acceleration voltage of the ion engine was pulsed on rapidly with all other thruster voltages and currents on and in steady state. Multiply charged species acquire an exhaust velocity proportional to $q^{1/2}$ where q is ion charge with a resultant separation of species in the initial TOF down the testing chamber. The ion current arriving at a distant collector has the general characteristics shown in Figure 3 (from Reference 2) (which has assumed only ++ and + species from the ion engine discharge). Separation of species, even if $Hg^{+++}$ is present, is extremely clean provided that variations in ion time-of-flight from one charge species to another are large compared to the acceleration voltage switch-on time ($\sim 1 \times 10^{-6}$ seconds).

While the pulsed beam technique utilized in these previous experiments operated successfully, it is believed some concern could be raised over possible changes in the discharge operating conditions for the manner in which the pulsed technique was applied. Although there is no evidence for ion engine alterations, changes in the discharge might, in principle, occur depending on whether ions arriving at the screen grid were subject to extraction and acceleration or were allowed to be intercepted by and terminated at that electrode. Accordingly, for this series of experiments a variation in the ion TOF technique was utilized. In this variation the ion engine discharge and ion flow operate continuously and pulsed voltages are applied to a small portion of the ion exhaust beam approximately 1 meter downstream from the exit plane. The ion current entering a small aperture in the analyzer is subjected to electric fields which prevent the ions from reaching the analyzer collector. When these fields are removed, the now unperturbed ion flow moves through the analyzer, with, again an identifiable separation of specie currents during the initial ion TOF in the analyzer. The requirement for a clean

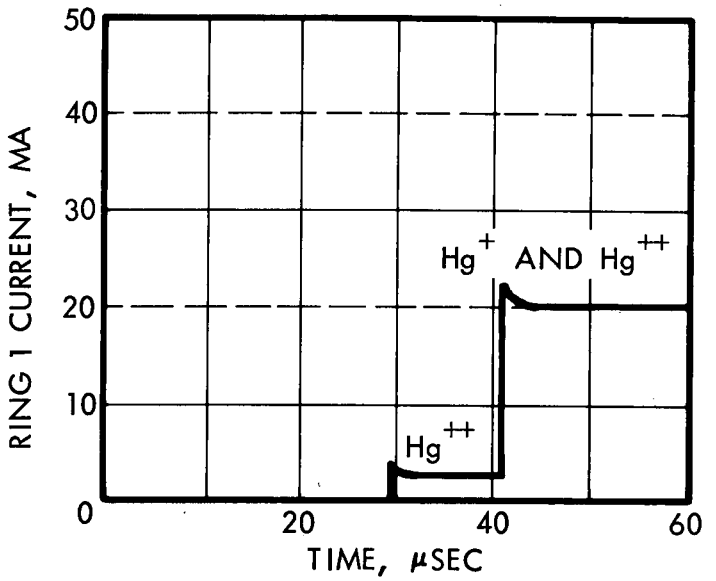


Figure 3. Representative Ion Current Signal to Collector Ring 1 in Pulsed Beam Tests After Acceleration Voltage is Pulsed on (t = 0). Beam Current component of $Hg^{++}$ arrives at ∿29 μsec after t = 0 while beam current component of $Hg^{+}$ arrives at ∿41 μsec, with ion time-of-flight proportional to $q^{-1/2}$ as predicted. Ratio of J++/J+ is ∿0.12, and relative abundance of ++/+ species is ∿0.06. No evidence of $Hg^{+++}$ for discharge conditions utilized. From Kemp, Sellen, and Pawlik[2]

separation of species is, in a manner similar to the previous TOF technique, that the switch-off time for the electric fields preventing ion passage in the analyzer be small compared to variations of ion TOF in the analyzer.

For the principle of ion TOF considered thus far, two major possibilities exist in the "perturbation" electric fields in the analyzer. In one configuration these electric fields are "longitudinal" and are oppositely directed to the ion flow. Figure 4a illustrates this configuration. With sufficient retarding potentials, the previously accelerated beam ions will come to rest and then be reflected backward toward the engine. Removal of the retardation voltage allows the ions to continue their flow into the analyzer and their eventual detection at the analyzer collector. This method presents several problems. The first of these is that the potential applied to analyzer electrodes must be such as to bring the accelerated ions to rest. For typical ion engine operating conditions, the ion acceleration voltage is ∿2000 volts and these potentials must also appear on the repeller grid in the analyzer. Such positive potentials,

a. LONGITUDINAL FIELD ION TOF ANALYZER

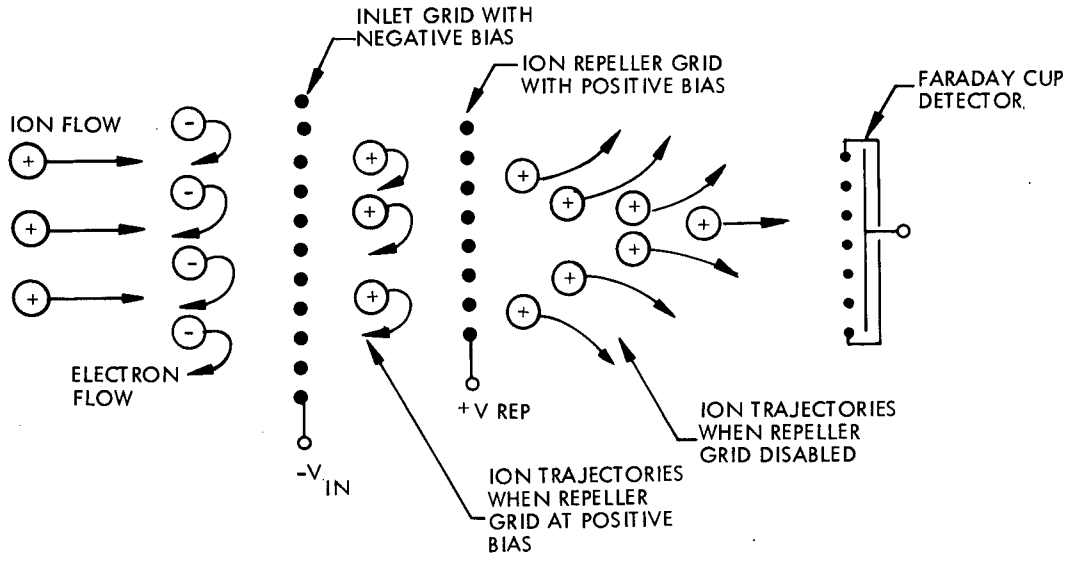


b. TRANSVERSE FIELD ION TOF ANALYZER

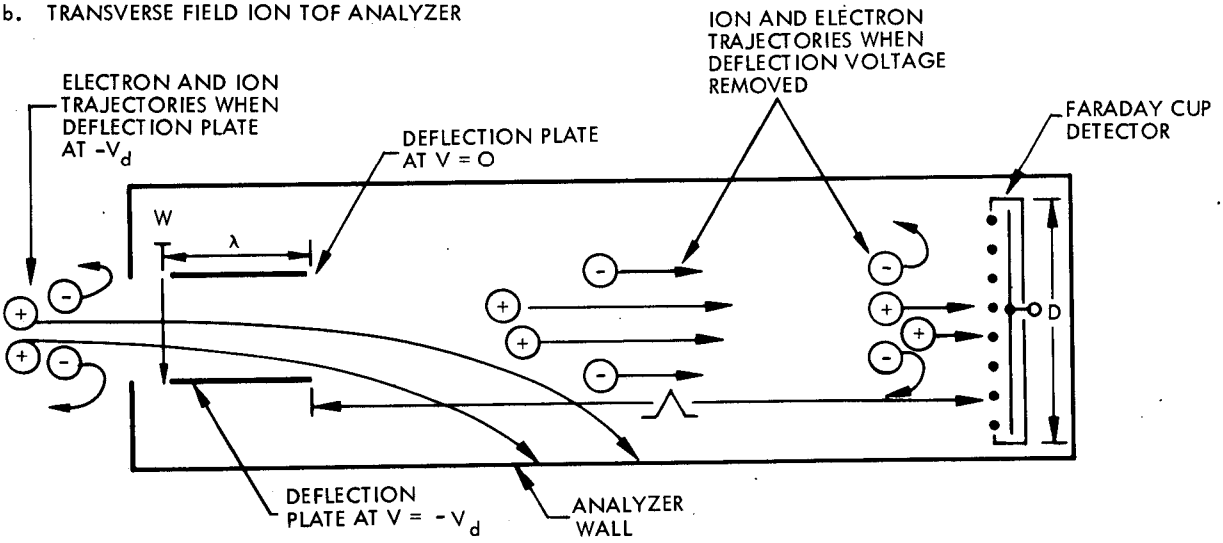


Figure 4. Operational Principles of Longitudinal and Transverse Field Ion TOF Analyzers

while repelling ions, attract electrons from the neutralized thrust beam and create electron drainage conditions which are highly disruptive to the beam neutralization. Accordingly, and to prevent electron drainage, an inlet grid on the analyzer must be used which will prevent electron entry into the analyzer, even in the presence of the comparatively strong attractive electric fields (for electrons) which exist due to the positive potentials on the ion repeller. The introduction of grids into the ion

flow, however, is, in general, a perturbing force. With the removal of the ion voltage on the repeller electrode, the ions may now proceed down the analyzer. However, electrons are still denied entry into the analyzer because of the inlet grid, and ions in the analyzer must proceed without the presence of neutralizing electrons. Since space charge forces in ion flows of this density are appreciable even for considerable downstream separations from the engine, ion beam expansion will occur in the analyzer with effects upon analyzer results which are difficult to assess.

The alternative arrangement of electric fields in an ion TOF analyzer is a "transverse field" analyzer (Figure 4b). In this configuration the ion flow enters an inlet channel which imposes an electric field perpendicular to the ion flow direction. The ion is deflected in this field and is either collected on one of the inlet plates or is allowed to intercept the wall of the analyzer. The removal of the deflection voltage allows the ions to proceed with unperturbed trajectories to the collector, with, again, charge specie currents separating on the initial TOF in the analyzer. Several advantages present themselves in this configuration. The first of these is that deflection of the ions can be accomplished, in general, with potentials that are small compared to those required for ion reflection. A second advantage is that there is no requirement for positive potentials to be applied to the deflection plates. Ion deflection can be achieved with one plate at zero potential (neutralized beam potential*) and the remaining plate at a negative voltage. Ions are attracted to the negative plate and electrons are repelled by it. Plasma flow in the presence of such negatively biased electrodes remains stable (whereas the flow becomes highly disturbed and unstable for positive voltages: for discussion of these effects see, for example, Reference 10). With the removal of the negative deflection voltage, the unperturbed plasma flow begins its passage through the analyzer. Because grids are not required at the analyzer input, electrons may now accompany the ions so that ion motion in the analyzer is unperturbed by unneutralized space charge forces. Separation of electrons from ions in the flow does occur eventually but only as a result of bias

*It is important to maintain all surfaces near the entrance aperture at this potential to minimize electrostatic "lens" effects which cause beam dispersion within the drift tube.

grids over the surface of the Faraday cup collector of the analyzer. From these several configurational advantages, a "deflection" type analyzer was chosen, rather than the "reflection" type.

## B. DEFLECTION VOLTAGE REQUIREMENTS IN A TRANSVERSE FIELD ION TOF ANALYZER

Figure 4b has illustrated a deflection channel of width w and length $\lambda$ with a deflection voltage, $V_d$, imposed across it. For an ion of mass, m, charge, q, and acceleration velocity, $v_+$, the action of the deflecting electric field is to give the ion a transverse velocity, $v_{tr}$, in its passage through the channel. Upon emerging from the deflection plates

$$v_{tr} = \frac{q\, V_d\, \lambda}{m\, v_+\, w} \tag{20}$$

and, since

$$v_+ = \left(\frac{2V_o}{m}\right)^{1/2}$$

where $V_o$ is the ion acceleration voltage, the angular deflection $\theta$ upon emerging from the deflection plates is

$$\theta = \frac{v_{tr}}{v_+} = \frac{\lambda V_d}{2wV_o} \quad . \tag{21}$$

A minimum requirement in the TOF analyzer is that an ion be deflected out of the Faraday cup at the end of the analyzer. For a cup of diameter D and with a deflector-to-collector separation of $\Lambda$, the minimum permissible value of $\theta$ is

$$\theta_{min} = \frac{D}{2\Lambda} = \frac{\lambda\, V_{d,min}}{2w\, V_o} \tag{22}$$

which yields

$$V_{d,min} = \frac{w\, D\, V_o}{\lambda\, \Lambda} \tag{23}$$

Note that this is independent of ion charge, q, which is a desirable feature.

Now, as an example of the voltages required for a practical case, consider w = 0.01m, D = 0.05m, $\lambda$ = 0.03m, and $\Lambda$ = 0.6m with $V_o$ = 2000 volts. Then $V_{d,min} \doteq 55$ volts which is $<< V_o$. Thus, only comparatively small deflection voltages are necessary for realistic experimental conditions in analyzer construction and ion energy. However, in practice it is desirable that ions be bent through angles which are larger than the minimum angle and, hence, result in interception on the analyzer support walls well in advance of the Faraday cup position to accommodate any beam dispersion. Also the above equations do not treat the effects of space charge on the required deflection voltage (discussed below). For both of these reasons additional deflection voltage will be required. Again, it is of interest to note that in the equations of motion, the ion charge q does not appear in the final ion trajectory. Thus, the transverse electrostatic deflection acts upon $Hg^+$ and $Hg^{++}$ in an identical manner, without the establishment of varying deflection requirements for the varying charge species.

The problems of "space charge loading" are introduced when realistic values of ion density are treated. [Equations (20) through (23) represent the flow of a single ion]. In order for a transverse electric field to act upon all ions, it is necessary for $V_d$ to exceed the potential buildup in an unneutralized slab of ions of charge density $\rho_+$ and thickness w. Using MKS units, this requires

$$V_{d,min} = \frac{\rho_+ w^2}{2\epsilon_o} \quad . \tag{24}$$

For example, an ion flow density of $10^{15}$ ions/$m^3$ (and assuming singly charged ions) and for w = 0.01 meter, then

$$V_{d,min} = 1.6(10)^{-19}(10)^{15}(10)^{-4}(2\pi)(9)(10)^9 \doteq 900 \text{ volts},$$

a voltage considerably in excess of that given from Equation (23)

Since the deflection requirement now includes the effects of ion space charge, it is of interest to evaluate this quantity. In the plane immediately following ion acceleration and for 1 ampere ion flow moving at $4 \times 10^4$ m/sec and a beam of diameter 0.2 meter, the ion density is

$\doteq 5 \times 10^{15}$ ions/$m^3$, which is five times larger than the example given above. The transverse deflection, then, is not appropriate if the analyzer is to be placed immediately downstream from the ion engine exhaust plane. However, because of angular divergence of the ion beam, the density at a point 1 meter downstream from the ion engine is reduced by an order of magnitude from its initial density. In these experiments the analyzer inlet was at 1 meter, where the requirement on $V_d$ due to space charge reduced to a value of $\simeq$ 450 volts for even the largest accelerated ion flows. In practice, values of $V_d$ employed ranged to $\sim$600 volts with the upper part of this range used for the highest levels of ion density.

A final area of concern is in requirements on switch-off time for the deflection voltage and in the separation ability of the TOF analyzer in the identification of charge species. Since the deflection channel has, of necessity, a non-zero length, $\lambda$, ions passing through it have a dwell time of $\frac{\lambda}{v_+}$. For $\lambda$ = 0.03 meter and $v_+ = 4 \times 10^4$ m/sec, this dwell time is approximately 1 microsecond.

Thus, removal of the deflection voltage instantaneously would lead to a portion of the flow $\sim$1 microsecond in duration which would possess varying "histories" of transverse acceleration within it. On the other hand, if the deflection voltage switch-off occurs over a period long compared to 1 microsecond, then the ion behavior downstream of the inlet channel will possess time variations mainly influenced by the switch-off. An acceptable switch-off criterion, then, is to make the switch-off time less than ion dwell time in the deflection channel and to require, finally, that ion dwell time in the inlet be small compared to variations in the ion TOF in the analyzer due to variations in ion charge and ion exhaust velocity. For a deflector-to-collector interspace of 0.6 meter and $v_+ = 4 \times 10^4$ m/sec, the $\tau_+$ (for $Hg^+$) is $\simeq$15 microseconds. The $\tau_{++}$ (for $Hg^{++}$) is reduced to $\simeq$10.5 microseconds (since $v_{++} = \sqrt{2}v_+$) and $\tau_{+++}$ is $\simeq$8.5 microseconds. The ion dwell time in the inlet channel of $\sim$1 microsecond is small compared to $\Delta(\tau_+ - \tau_{++})$ of 5 microseconds, but is of comparable magnitude to $\Delta(\tau_{++} - \tau_{+++})$ of 2 microseconds. Therefore, separation of $Hg^{++}$ from $Hg^+$ should be well defined while separation of $Hg^{++}$ and $Hg^{+++}$ would be marginal in the present system. However, from

the earlier measurements of Reference 2, the "appearance" potential in anode discharge voltage for $Hg^{+++}$ production is considerably above the parameter range for present ion engine operation. If, however, conditions should alter somehow so as to require these higher anode voltages and if the $Hg^{+++}$ presence were of concern, the ion TOF configuration could be suitably altered to determine $Hg^{+++}$ by increasing $\Lambda$ or by decreasing $V_o$, the ion engine acceleration voltage. For the purposes of the present experiment, good separation of $Hg^{++}$ and $Hg^{+}$ was achieved with an analyzer drift space of 0.6 meter and an inlet channel length of 0.03 meter, deflection voltages of less than or equal to 600 volts, and switch-off times of less than 1 microsecond.

## C. ION TOF ANALYZER CONSTRUCTION AND OPERATION

The values of $\lambda$, $\Lambda$, w, and D have been previously specified, while Figure 4b has illustrated these quantities relative to the ion flow. Figures 5 and 6 show portions of the completed probe. In Figure 7 the arrangement and range of angular positions of the probe relative to the ion engine may be seen.

Figure 8 illustrates the timing sequence for the switch-off of the acceleration voltage and Figure 9 shows oscilloscope traces with indicated arrivals and abundances of the $Hg^{++}$ species and the $Hg^{+}$ species. After these initial experiments, the TOF analyzer was then applied to the series of experiments described in the following section.

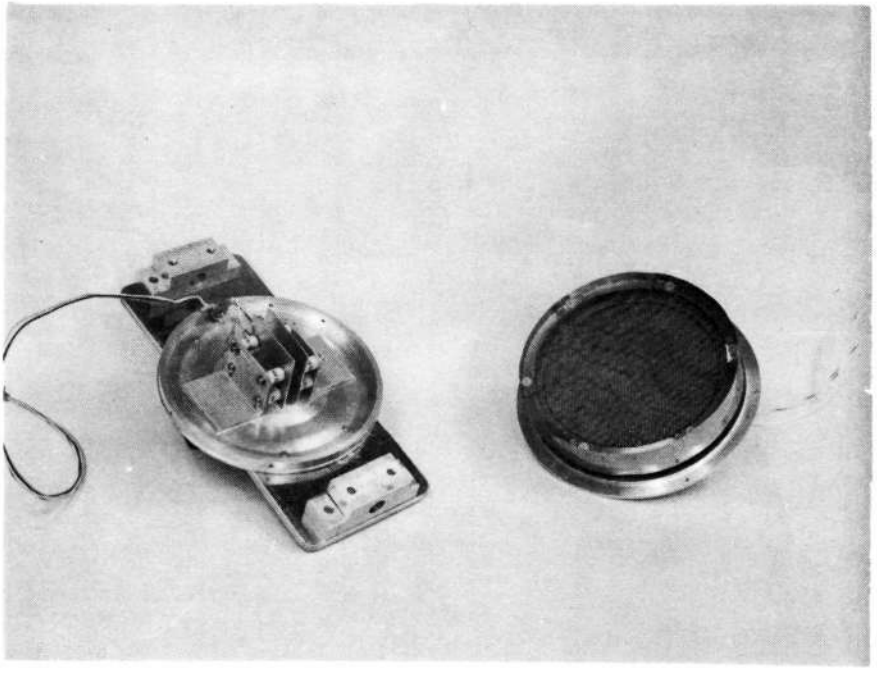

Figure 5. Deflection Plate Assembly and Faraday-Cup Assembly of the TOF Probe

Figure 6. Completely Assembled Time-of-Flight Probe for Measurement of $Hg^{+}$ and $Hg^{++}$ Ion Abundances. The figure shows the 1 x 3 cm ion entrance aperture and clamps which affix the probe to the support structure.

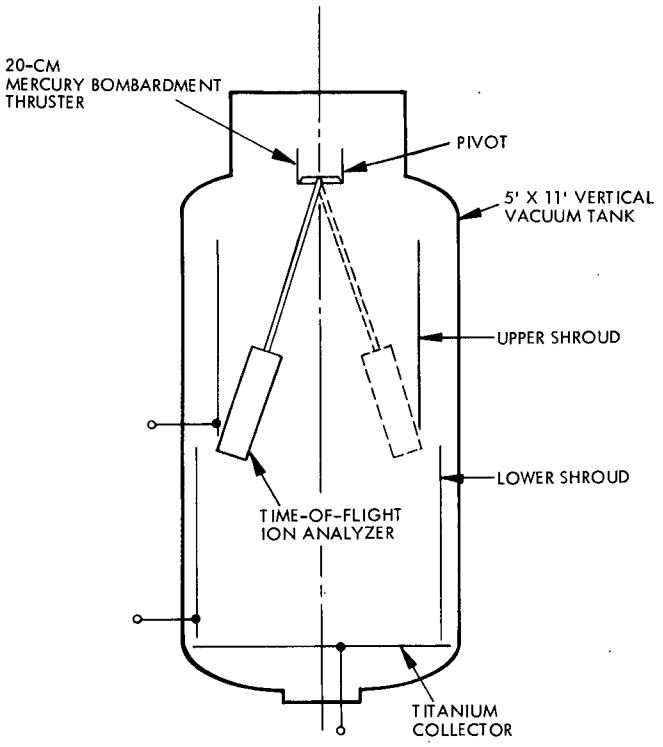


Figure 7. Arrangement of Ion Engine and TOF Probe in Vacuum Tank.

Engine projects beam vertically downward. Probe entrance is 1 meter from engine accelerator grid. Maximum swing of probe is ± 18 degrees.

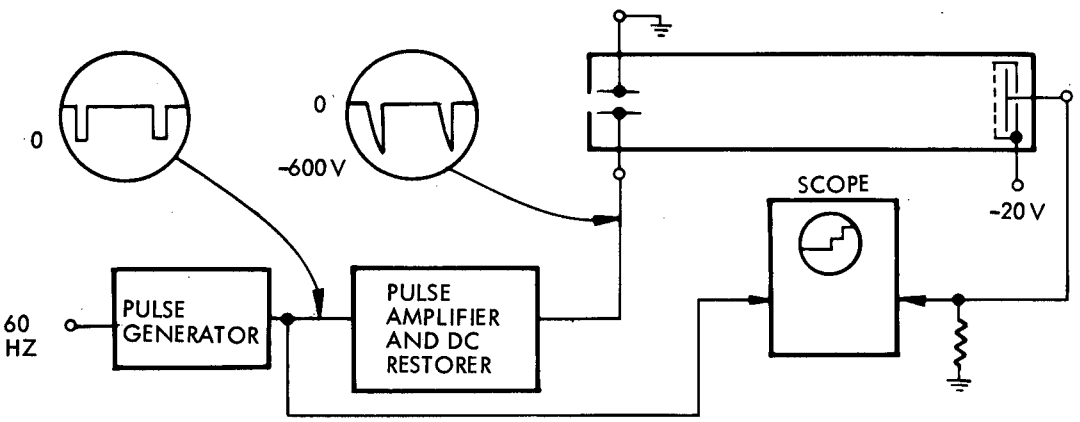


Figure 8. Pulsing Arrangement for the TOF Probe.

Trigger pulses are generated 60 times per second. Measurements are made during the first several microseconds following the positive step in deflection plate voltage.

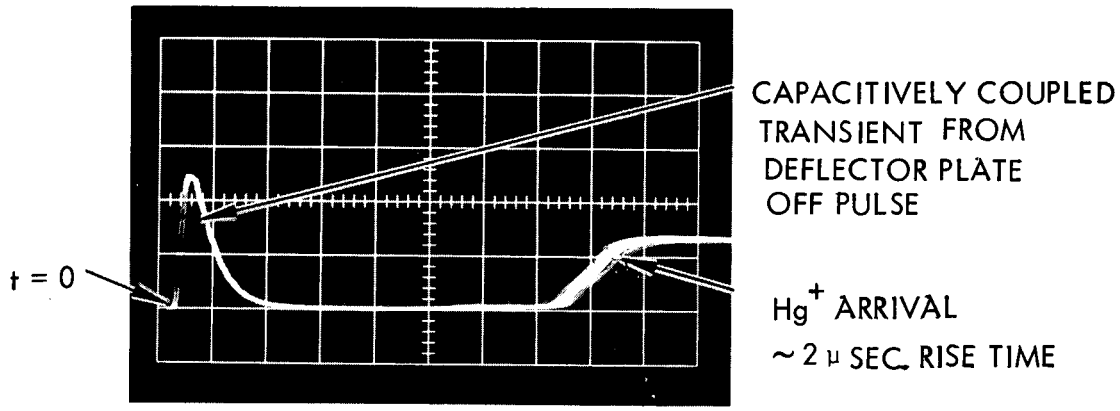


Figure 9a. Ion TOF Collector Signal. Oscilloscope Sensitivity 0.020 Volt/Division Across 1 KΩ Vertical and 2 μSec/Division Horizontal.

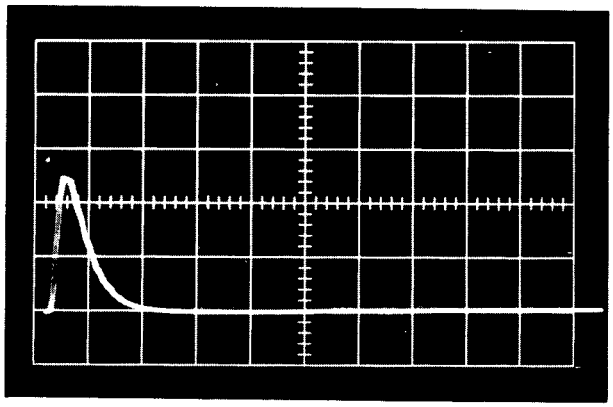

Figure 9b. Ion TOF Collector Signal With No Ion Beam. Capacitively Coupled Transient Still Evident But Signal Noise at Later t (>10 Sec) is Less Than Trace Width.

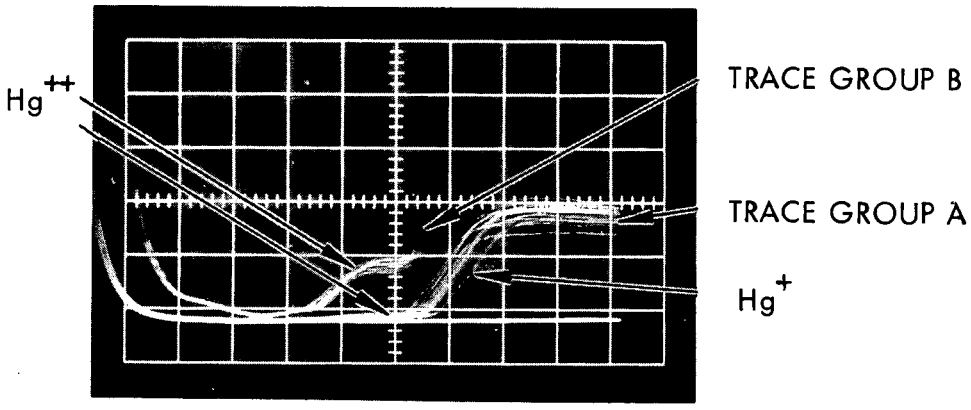


Figure 9c. Ion TOF Collector Signal. Oscilloscope Sensitivity 0.010 Volt/Division (Trace Group A) and 0.001 Volt/Division (Trace Group B) Across 1Ω Vertical and 2 μSec/Division Horizontal.

# IV. $Hg^{++}/Hg^{+}$ EXPERIMENTS

## A. ++/+ RATIO AS A FUNCTION OF ANODE VOLTAGE AND ION BEAM CURRENT

From the previous qualitative analysis of Section II, the most important parameters in the ++/+ ratio may be expected to be the anode voltage (which establishes the nature of the discharge electron energy distribution) and the electron density in the discharge. Measurements of the ++/+ ratio as a function of anode voltage are comparatively simple to obtain. In contrast, direct measurements of discharge electron density are difficult to obtain and assess since they require insertion of probes within the discharge chamber with resulting alterations of the discharge properties. Therefore, alternative means of establishing ++/+ dependence on discharge electron density was sought. The method which appeared most promising was to examine the ++/+ ratio as a function of ion beam current.

The ion beam current is roughly given by

$$I_b \doteq q n_{+d} \bar{v}_{+d} A_{sg} \tag{25}$$

where $I_b$ is ion beam current, $qn_{+d}$ is ion density in the electron bombardment discharge, $\bar{v}_{+d}$ is effective ion drift speed toward the screen grid and $A_{sg}$ is screen grid aperture area. Since the plasma discharge is highly neutralized throughout most of its volume ($n_+ = n_e$), then $I_b$ is proportionally related to $n_e$.

Furthermore if $I_b$ may be varied without varying the anode potential (for example, through variations in propellant injection rate), then variations in $I_b$ presumably occur without significant shifts in effective ion drift velocity, $v_{+d}$, or in the acceptance area or ion transmission by the screen grid. Hence

$$I_b \doteq k\, n_e \Big|_{V_{\text{anode fixed}}} \tag{26}$$

provided that the restrictions outlined above are upheld.

Figure 10 illustrates the ratio of ++/+ ion currents in the ion beam as beam current and anode voltage are varied. Figure 11 is a cross plot of the data in Figure 10. Since the current contribution of an $Hg^{++}$ ion is twice that of an $Hg^{+}$ ion, the ++/+ current ratio is a factor of two larger than the ++/+ abundance ratios utilized throughout the analyses [Equations (12) through (18)]. Conversion between the two ratios is considered sufficiently simple so that both current and abundance expressions of these ratios will be retained.

Figure 10 has several prominant features which merit discussion. The first of these is the "appearance potential," in anode voltage, for $Hg^{++}$ production. The double ion content is clearly evident at anode voltages of 25 volts and from extrapolations in the cross-plotted data of Figure 11, $Hg^{++}$ becomes measurable at anode potentials of ∿21 to 23 volts. Since it is unlikely that electrons in the discharge have kinetic energies in excess of the cathode to anode potential difference, the presence of $Hg^{++}$ at these anode settings clearly evidences sequential ionization as a contributor to the overall $Hg^{++}$ production. (The threshold for $e + Hg^{o} \rightarrow Hg^{++} + e + e$ is ∿30 electron volts, while $e + Hg^{+} \rightarrow Hg^{++} + e + e$ has a threshold of ∿19 electron volts.) Pawlik et al[4] also observed a threshold anode potential of ∿21 volts for $Hg^{++}$, and concluded that ionization to $Hg^{++}$ occurred from other than the $Hg^{o}$ ground state. This possibility is discussed below. The data of Milder[1] also evidenced an onset of $Hg^{++}$ at anode voltages of ∿20 volts.

Two possible two-step reactions for the production of $Hg^{++}$ may be advanced. The first of these is sequential ionization ($e + Hg^{o} \rightarrow Hg^{+} + e + e$, $e + Hg^{+} \rightarrow Hg^{++} + e + e$). It is also possible to produce $Hg^{++}$ through ionization of metastable $Hg^{o}$. THe 6 $^{3}P_{2}$ and 6 $^{3}P_{0}$ states are metastable with excitation levels of 5.4 ev and 4.7 ev, respectively, which may be subsequently doubly ionized by a single electron impact. The energy threshold for this reaction is ∿25 electron volts. However, the magnitude of processes involving removal of two electrons by a single electron impact remains very small until electron energy is considerably above threshold (see,[11] for example, $e + Hg^{o} \rightarrow Hg^{++} + e + e$), so that $Hg^{++}$ from a single stage charge transfer from metastable $Hg^{o}$ is unlikely at 25 volts, and, energetically impossible (for the $^{6}P$ states) at 21 volts. In summary

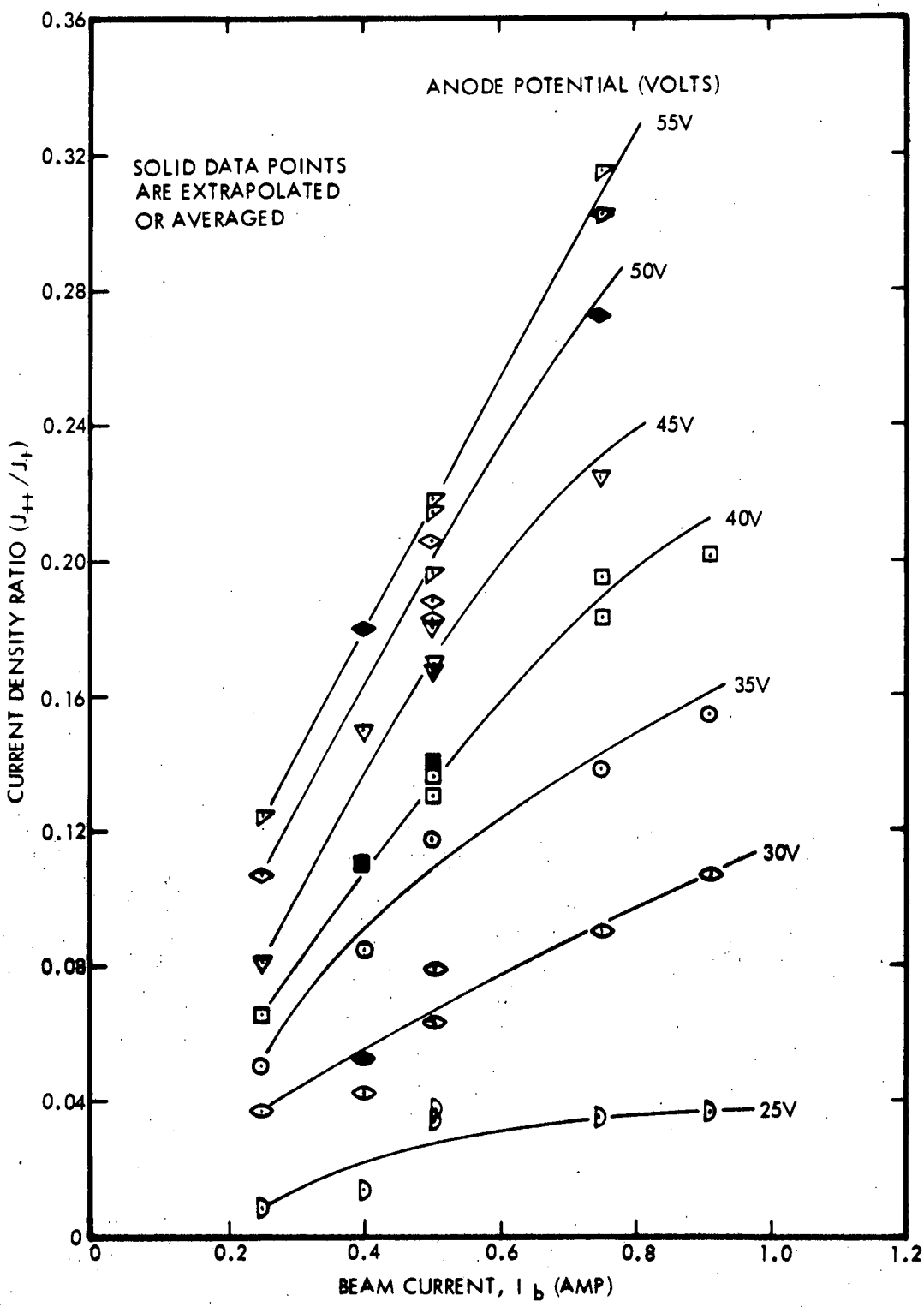


Figure 10. Doubly to Singly Charged Ion Current Density Ratio as a Function of Beam Current with Anode Voltage as a Parameter

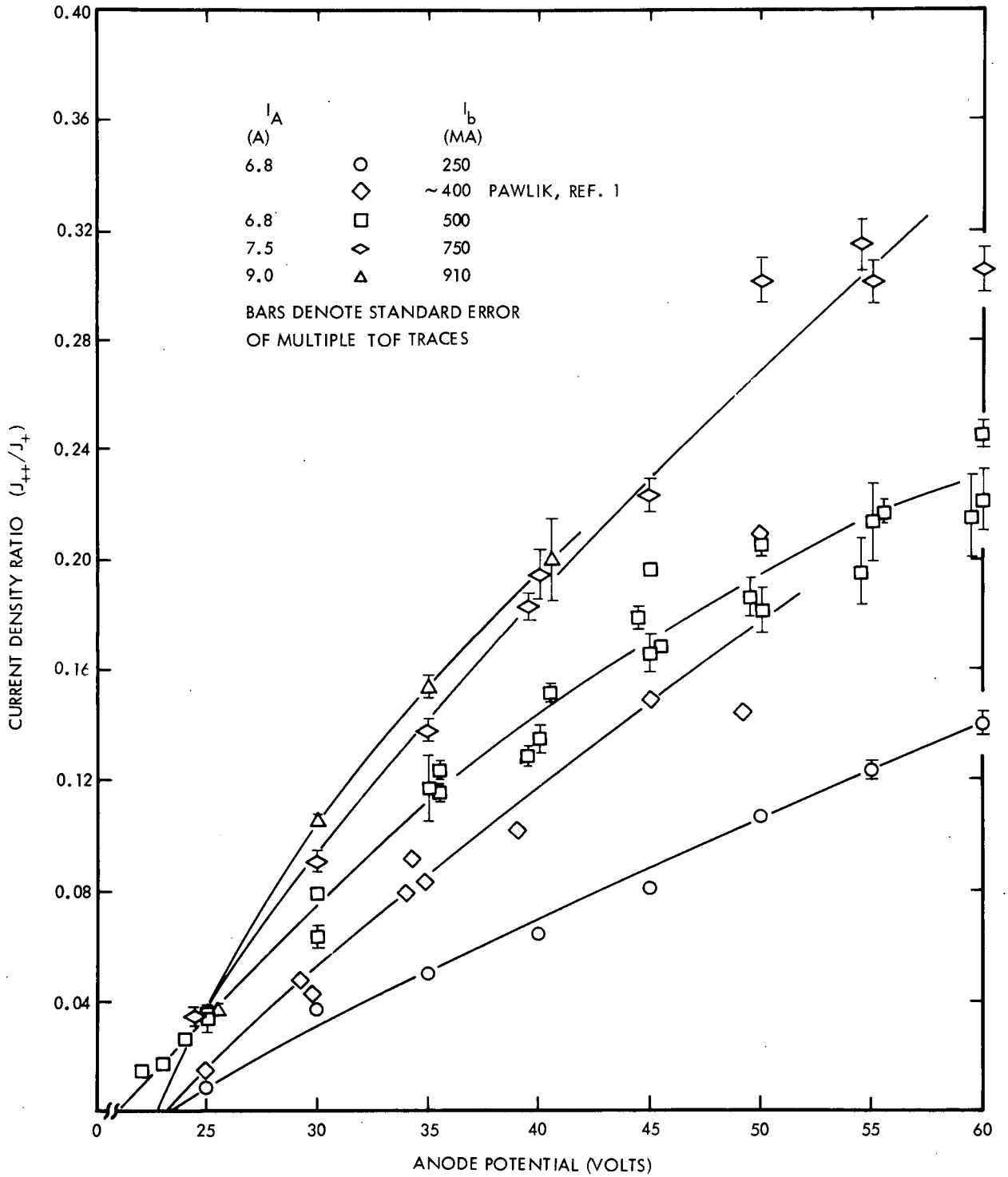


Figure 11. Doubly to Singly Charged Ion Current Density Ratio as a Function of Anode Potential with Beam Current as a Parameter

to this point, the threshold data in Figures 10 and 11 are strong indications for the production of $Hg^{++}$ by a sequential ionization process from $Hg^{o}$ to $Hg^{++}$.

A second feature to note in Figure 10 is the behavior in $J_{++}/J_{+}$ as a function of beam current for fixed anode voltage. From Equation (26), $I_b$ is proportional to $n_e$ under certain discharge restrictions. Also, from Equation (14), the abundance of ++/+ is essentially linear in $n_e$ provided that $n_e F_{12} T$ is the predominant term in the numerator. Thus, the ++/+ ratio might be expected to be essentially proportional to $I_b$. The data in Figure 10 clearly reveal abundance ratios with, essentially, linear dependence upon $I_b$. As pointed out in the discussion of Equation (14), experiments revealing a ++/+ dependence on $n_e$ at fixed electron energy are strong evidence for sequential ionization.

A final point to examine in the data in Figures 10 and 11 is the dependence of the ++/+ ratio, as anode potential is varied for a fixed level of beam current. As may be noted, the ++/+ ratio increases with increases in anode potential for all levels of beam current. For fixed beam current, the values of $n_e$ and T in Equation (19) may be expected to remain relatively invariant, yielding the further approximation

$$\left.\frac{\partial(++/+)}{\partial V_{anode}}\right|_{I_b \text{ fixed}} \simeq k\, I_b \left(\frac{\partial F_{12}}{\partial V_{anode}}\right)_{I_b \text{ fixed}} \qquad (27)$$

where k is a constant and $I_b$ is beam current.* In examining the data of Figure 11, the $J_{++}/J_{+}$ ratio would appear to indicate that $\frac{\partial F_{12}}{\partial(V_{anode} - 22 \text{ volts})}$ is approximately a constant so that one may write

$$(++/+) \simeq k'\, I_b\, (V_{anode} - 22) \qquad (28)$$

where again, k', is a constant. It should also be emphasized that the analysis here has focused entirely on $F_{12}$ as the process through which

*Note, $n_e F_{12} T \ll 1$.

the doubly charged ion appears. This is considered a valid assumption in view of the estimates of $F_{02}$ derived from the (limit $n_e \rightarrow 0$) process previously described.

B. ++/+ RATIO AS A FUNCTION OF ION ACCEL-DECEL VOLTAGE

The experimental data points given in Figures 10 and 11 were obtained with a voltage of +2 kv on the screen grid and with -1 kv on the accelerator grid. The plasma thrust beam potential was 0 volt so that accelerated ions possessed 2 kev of kinetic energy. In principle the accel and decel voltages should not be of consequence in the ++/+ ratio. Ions formed in the discharge drift to the forward sheath of the plasma and are then accelerated by the applied voltage. Acceleration fields do not penetrate into the discharge plasma and, hence, should not affect discharge processes. The extent of ion deceleration following acceleration should also be of no consequence to discharge processes since the decel fields also do not penetrate into the electron bombardment plasma. To test this concept, the $J_{++}/J_{+}$ current ratio was determined for a constant 3 kv potential between the screen grid and the accel grid as the accel grid potential was varied from -1.0 to -2.0 kv, thus varying the ratio of final ion energy to decel potential from 2.0 to 0.5, a variation of a factor of 4. The results of this experiment are given in Figure 12. The measured current density ratio remained essentially constant at 0.12 as expected. Moreover, it is in agreement with the results of Pawlik et al[4] for similar variations in $V_{-}$ and $V_{+}$. In summary to this experiment, abundances of ++ and + ions are not dependent upon ion deceleration fields.

C. ++/+ RATIO AS A FUNCTION OF DIVERGENCE ANGLE FROM THE THRUST BEAM AXIS

The experimental data points of Figures 10, 11, and 12 were all obtained with the ion TOF analyzer on the axis of the thrust beam. Through its mounting arms the TOF analyzer may be moved through the beam. During this motion, the TOF analyzer axis continues to be directed at the center of the ion engine exit plane so that the entering ion flow remains directed along the analyzer axis. The test chamber limits the motion to angles of $\pm$ 18 degrees with respect to the beam axis, but this incorporates a very large fraction of the total ion beam. When $J_{++}/J_{+}$ was measured as the

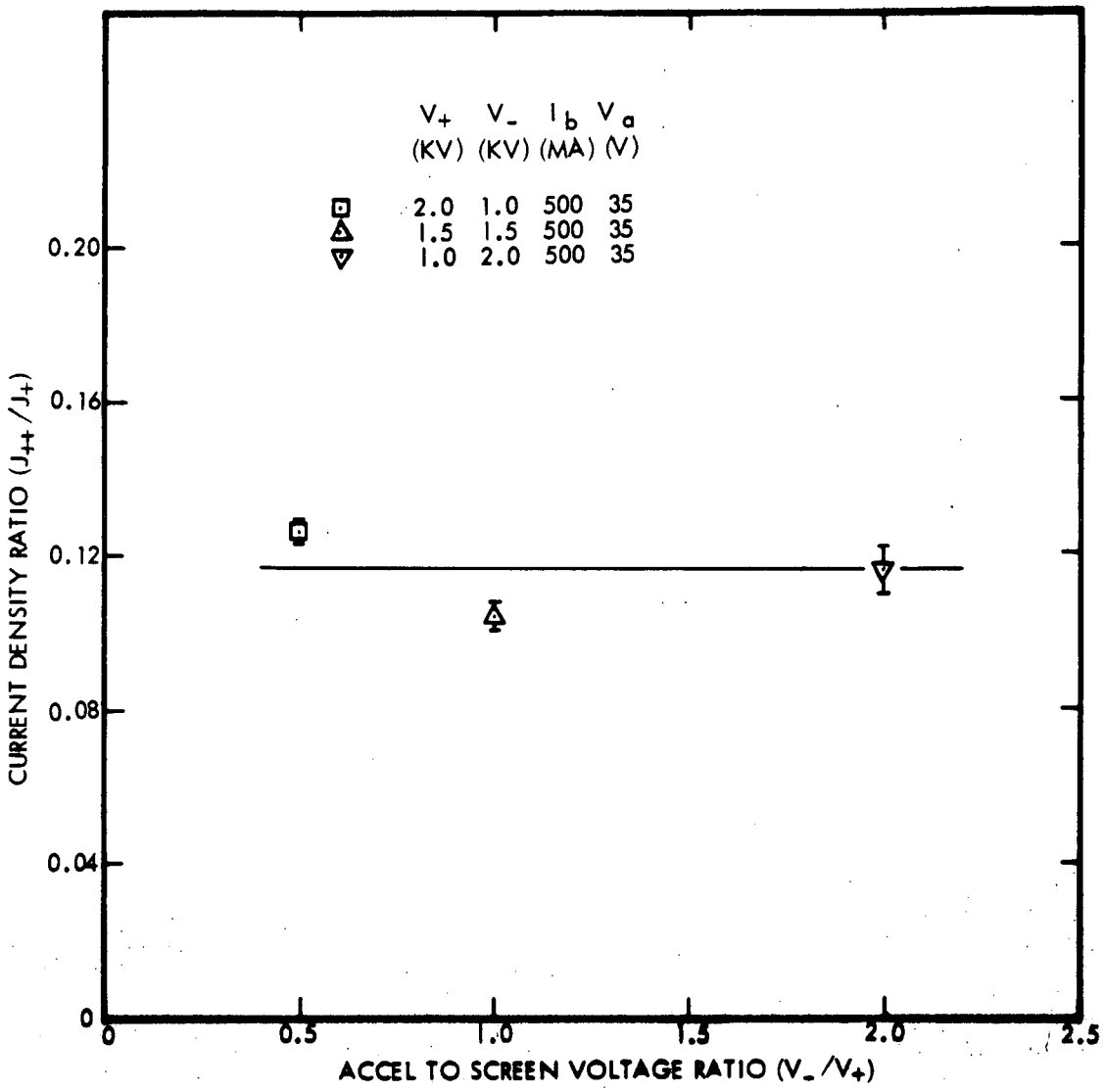


Figure 12. Doubly to Singly Charged Ion Current Density Ratio as a Function of Accel-to-Screen Electrode Voltage Ratio

analyzer moved from the beam axis to angles of 15 degrees from the beam axis, the current ratio remained invariant (Figure 13). This result was an expected one, since the emergence and distribution of doubly charged ions relative to the beam axis should be identical to that of singly charged ions, as discussed below.

If one examines the trajectory of both charge species in moving from the plasma discharge to the neutralized beam flow, the radius of curvature of a specific charge species is given by

$$R = \frac{Mv^2}{qE_\perp} = 2q(V_{dp} - V)/qE_\perp \qquad (29)$$

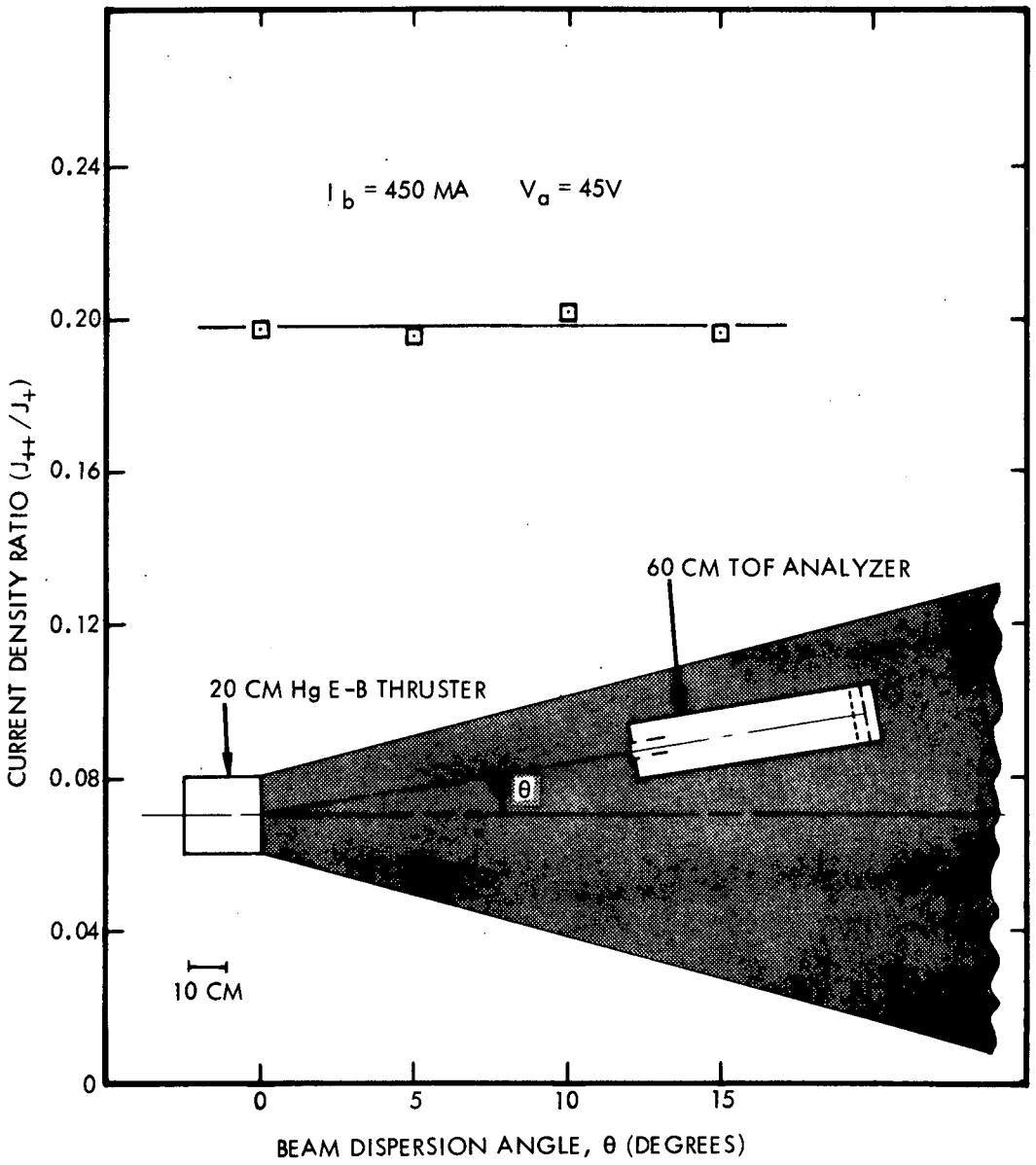


Figure 13. Doubly to Singly Charged Ion Current Density Ratio as a Function of TOF Analyzer Position Angle

where q is particle charge, $V_{dp}$ is the potential in the discharge at which the ion originated, V is the potential at the point in question, and $E_\perp$ is the electric field perpendicular to the trajectory at the point in question. Since q appears in both the numerator and denominator of Equation (29), the particle trajectory is charge invariant. This trajectory invariance has been previously treated in Section III dealing with transverse field deflection in the ion TOF analyzer. Thus, measurements made on the axis of the beam are representative of the ion beam as a whole, as demonstrated in Figure 13.

## D. ++/+ RATIO AS ELECTRON BOMBARDMENT DISCHARGE PARAMETERS ARE VARIED

In Section IV-A experimental results were presented and compared to the predictions of a qualitative analytical model of the discharge. In general, agreement is comparatively good, and suggests that at least a parametric description of the discharge operation may be obtained from the simple analytical model. The discussion has also presented some cautionary emphasis regarding use of the simple analysis. This is particularly true if a specific variation in the discharge should affect the population of more energetic electrons in the discharge. Considering that the principal source of doubly charged ions is through sequential ionization, processes that affect $F_{12}$ must be treated with some care. Recalling Equation (8)

$$F_{12} = \int_0^\infty f_e(E)\, v_e\, \bar{\sigma}_{12}(E)\, dE \qquad (8)$$

it may be seen that $F_{12}$ is sensitive to the "overlap" between $f_e$ and $\bar{\sigma}_{12}$ and, since transitions from the first to the second ionized state require electrons with energies in excess of 19 electron volts, discharge processes that prevent significant electron populations above 19 ev may drastically alter the production of $Hg^{++}$. Such variations that affect $Hg^{++}$ production may not be significant in $Hg^{+}$ production since overlap between $f_e$ and $\sigma_{01}$ requires only an electron population above ~11 ev.

To illustrate the variations that may be introduced into the ++/+ ratio, a series of three experiments was performed with the 20-cm-diameter thruster. For all three conditions the screen voltage was maintained at +2000 volts with the accelerator grid at -1000 volts. Mercury throughput

to the engine was held essentially constant, and since a high value of propellant utilization yields the beam current of 0.75 ampere in Case 1, below, the utilization in Cases 2 and 3 is substantially reduced.

Table 1. Variation of Propellant Utilization

| Case and Conditions | $I_{beam}$(amp) | $J_{++}/J_{+}$ | $\Sigma$ | $\eta$ |
|---|---|---|---|---|
| 1. ($V_{anode}$ = 35 volts, $I_{anode}$ = 7.5 amperes, $I_{magnet}$ = 0.65 ampere) | 0.75 | 0.1780 | 0.0163 | >0.90 |
| 2. ($V_{anode}$ = 34 volts, $I_{anode}$ = 2.5 amperes, $I_{magnet}$ = 0.65 ampere) | 0.45 | 0.0047 | 0.0013 | ≈0.55 |
| 3. ($V_{anode}$ = 35 volts, $I_{anode}$ = 5.2 amperes, $I_{magnet}$ = 0.25 ampere) | 0.55 | 0.0138 | 0.0032 | ≈0.70 |

Column $\Sigma$ in Table 1 is the standard variation for the experimental values of $J_{++}/J_{+}$ listed for each case. From the results obtained it is evident that large variations in $J_{++}/J_{+}$ may occur, under certain circumstances, for only modest variations in thruster operating conditions.

In the discussion of a previous section, (IV-A), an approximate relationship of

$$(++/+) \cong k' I_b (V_{anode} - 22) \qquad (28)$$

was introduced as representative of much of the experimental data. To illustrate the adequacy of this expression, values of

$$k' = (J_{++}/J_{+})/I_{beam} (V_{anode} - 22)$$

are given in Figure 14 for beam currents ranging from 0.25 to 0.90 ampere and anode voltages from 25 volts to 55 volts. It may be noted that variations in k' in Equation (28) are comparatively small while the quantity

$I_b$ ($V_{anode}$ - 22) varies well over one order of magnitude. Even those observed variations in the calculated value of k' could be reduced by variations in the magnitude of the chosen "threshold anode voltage" (the 22 volts used above) by only one volt or so. However, the figure of 22 volts drawn from apparent thresholds in Figure 11) is not defined within 1 or 2 volts. Equation (28) is only a parametric expression of observed engine behavior, and minimizing variations in some apparent k' in Equation (28) is beyond the accuracy or intent of the analysis. What is of importance is to recognize the generally valid linear relationship of $J_{++}/J_+$ to the product of beam current times an anode voltage minus a threshold potential.

When the data points of Cases 1, 2, and 3 of Table 1 are placed on Figure 14, it may be noted that Case 1 is in general agreement with the "conventional" relationship of $J_{++}/J_+$ and $I_b(V_{anode} - 22)$ while Cases 2 and 3 are markedly different. It will be advanced here that these variations are the result of variations in $f_e$ under conditions of essentially fixed anode potential.

To produce the operating discharge of Case 2, all engine parameters remained at fixed values except that anode current (electron bombardment current) was reduced to 2.5 amperes. Nominally this discharge current is an order of magnitude larger than beam current, a condition which insures a "thick" discharge to single ionization and a high propellant utilization. When this anode current diminished to values of only $\sim$5 times beam current, the propellant utilization was "spoiled" (diminished to $\sim$0.5). However, while $I_b$ ($V_{anode}$ - 22) only diminishes by a factor of 2 from Case 1 to Case 2, the $J_{++}/J_+$ ratio diminished by $\sim$40. The only apparent source for such radical behavior would appear to be that the population of $f_e$ above the threshold for sequential ionization has been altered from Case 1 to Case 2. While $n_e$ and $f_e$ can remain sufficiently high so that approximately half of the injected neutrals are moved from the ground state to the first ionized state, the overlap between $f_e$ and $\bar{\sigma}_{12}$ can vary dramatically because of the major variations in $\bar{\sigma}_{12}$ moving away from threshold.

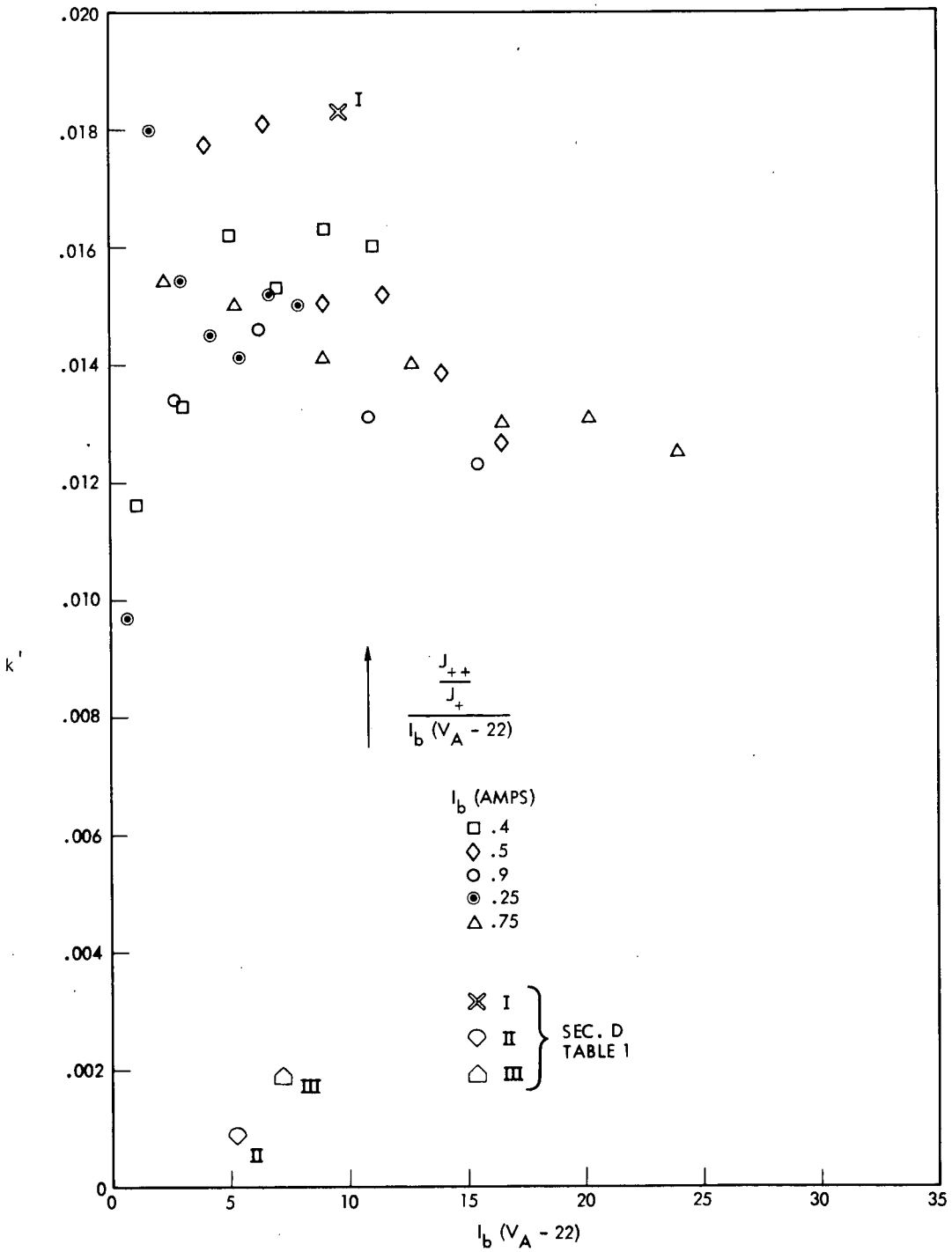


Figure 14. Value of Proportionality Constant k' in $J_{++}/J_+ = k'I_b(V_A - 22)$. Values are for $I_b$ ranging from 0.25 to 0.90 ampere and $V_A$ ranging from 25 to 55 volts. k' is approximately 0.015 $\pm$ 0.002 for $I_b(V_A - 22)$ ranging from $\sim$2 to $\sim$24 watts. Cases I, II, III represent other discharge conditions, both "on-line" (I, high propellant utilization) and off-line (II and III, spoiled propellant utilization) operational conditions.

In moving from Case 2 to Case 3, the anode current was increased from 2.5 to 5.5 amperes and magnet current was diminished from 0.65 ampere to 0.25 ampere. These effects might be expected to be counteracting in their effects on the population of $f_e$ in energetic electrons, since increases in electron bombardment current should increase the abundance of energetic electrons in the discharge while diminutions in magnetic fields should allow a more rapid transport of fast electrons to the anode with a subsequent loss of population of $f_e$ in energetic states. If such counteraction is, indeed, present, it may explain the observed values of doubly charged ions, since $J_{++}/J_+$ remains an order of magnitude below the "conventional" level, even for relatively high values of discharge parameters ($I_{anode}$ = 5.5 amperes, $V_{anode}$ - 22 = 13 volts).

While the results of Cases 2 and 3 and the explanations advanced here do not explore exhaustively or explain rigorously all discharge behavior, they do suggest that the value of the ++/+ ratio may be utilized as a sensitive "probe" of the overall discharge. In this possible approach to discharge diagnosis, the injected neutrals act as probes, with the final abundance ratios of singly and doubly charged ions being a complicated but sensitive integral of the "history" of the "probing" particle in its passage through the discharge. Possible extensions of such techniques could utilize additional "tracer" elements, specifically selected for their properties for onsets at various ionization levels and electron energies. While the present program has not pursued these possibilities in depth, it has attempted one further experiment in $J_{++}/J_+$ as anode current is varied for fixed anode voltage and beam current.

Figure 15 illustrates $J_{++}/J_+$ as $I_{anode}$ decreased from 7.5 amperes to 3.0 amperes, and with $V_{anode}$ at 40 volts. Through the region 4.5 amperes $\leq I_A \leq$ 7.5 amperes, $J_{++}/J_+$ remained fixed at $\sim$0.15 [k' of Equation (28) = 0.017 watt$^{-1}$ in general agreement with the "on-line" operation of Figure 14]. However, as $I_{anode}$ diminishes to values less than $\sim$10 $I_b$, the discharge appears to "cool" sufficiently so that ++ production is inhibited. This observed behavior is also consistent with Case 2 of Table 1 (where the $V_A$ = 34 volts is somewhat lower than the $V_A$ = 40 volts

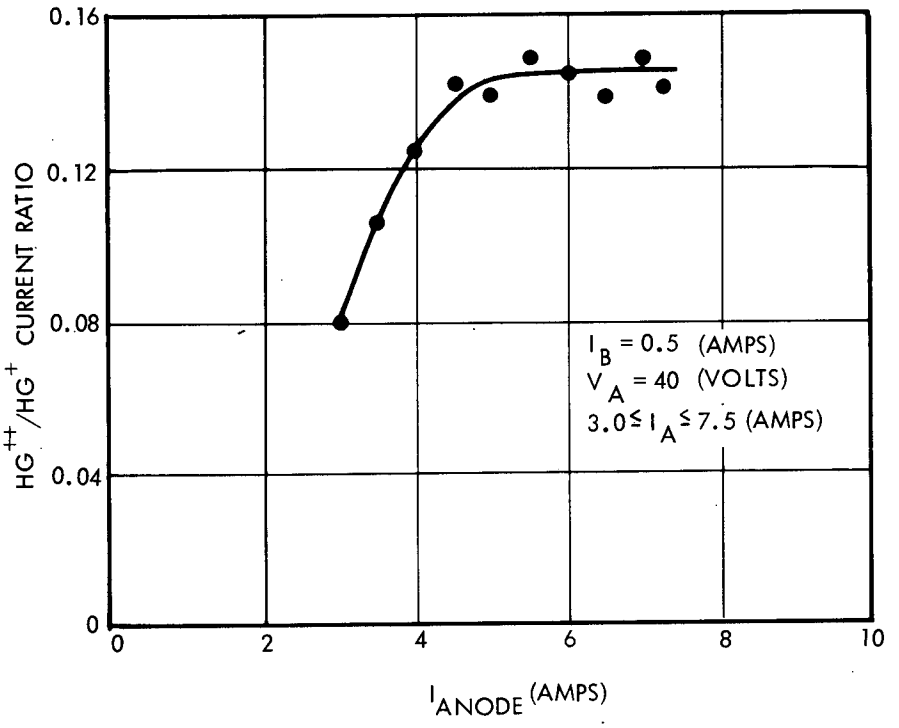


Figure 15. The $J_{++}/J_{+}$ Ratio as a Function of Discharge Current. Beam current, anode potential, and other operating parameters were held fixed.

of Figure 15). From Figure 5, it is apparent that good propellant utilization may be obtained with diminishing fractions of doubly charged ions, by suitable reductions in anode current. Below certain discharge current levels, however, the discharge becomes noisy and may be unsatisfactory for other reasons relating to ion engine impact upon spacecraft performance.

The data of Figure 5, and that of Figure 10 and Table 1 are also of interest to the point that they suggest that electron density in the ion engine discharge is not closely coupled to electron bombardment current (at least, for high propellant utilization discharge conditions). If beam current is, indeed, related to discharge electron density as suggested in Equations (25) and (26), then electron density in the discharge for the data of Figure 15 remained essentially constant as anode current varied over a factor of $\sim$2.5 (here propellant injection remained fixed). In Figure 10, variations in beam current of a factor of 4 were obtained with anode current and voltage fixed and variations in the neutral injection rate.

A final area for comment on the data in this and the preceding portions of Section IV is in the apparent threshold for ++ production. From Figures 10 and 11, it would appear that anode voltages of $\sim$22 volts are required for the onset of ++ production. Presumably electrons in the discharge may acquire kinetic energies as large as $eV_{anode}$. However, electrons in the discharge are first present in the region between the hollow cathode and keeper and then move into the main discharge chamber. In a separate series of experiments investigating electron temperatures in the plumes of hollow cathode plasma bridge neutralizers, it has been found that electrons have energies which are small compared to $e(V_{keeper} - V_{cathode})$. This suggests that the plasma densities in these hollow cathode discharges are sufficiently dense that electrons are in collisionally dominated transport, losing energy to collisions with atoms and ions and gaining energy from the electric field. In this manner an electron leaving a surface at $V_{cathode}$ may eventually dwell in a plume at $V_{keeper}$ and may only acquire a kinetic energy which is small compared to the indicated differences in potential. In this same manner, electrons in the ion engine discharge may reach the keeper region with only thermal energies of fractions of ev. Their subsequent entry into the main discharge may be sufficiently collisionless to allow rapid acquisition of kinetic energy but the maximum possible electron energy would then be $\approx e(V_{anode} - V_{keeper})$. When the keeper potential of 3 volts is included, then the earlier expression in Equation (28) utilizing $(V_{anode} - 22)$ volts may be rewritten as $[(V_{anode} - V_{keeper}) - 19]$ volts, which may be again rewritten to $[(V_{anode} - V_{keeper}) - V_{12,threshold}]$ where $V_{12,threshold} \approx 19$ volts is the known energetic threshold for sequential ionization of $Hg^+$. It has been previously suggested by Pawlik[12] that the important parameter in the study of ++ production may be $(V_{anode} - V_{keeper})$. The apparent onset of ++ production for $V_{anode} - V_{keeper} \doteq V_{12,threshold}$ presents interesting possibilities, both in explanation of observed ++ production, and, (referring to previous considerations of ++ production as a "probe" of plasma discharge behavior) as an element of ion engine discharge diagnosis.

## V. DISCUSSION AND SUMMARY

The ion TOF probe results have indicated a threshold anode potential of approximately 22 volts for the appearance of $Hg^{++}$. This is in qualitative agreement with the early data of Milder[1] for a somewhat different form of electron bombardment discharge, and is in good agreement with the data of Pawlik et al[4] for an identical 20-cm bombardment thruster. The 22-volt appearance potential for $Hg^{++}$ is strong evidence that the doubly charged ion results from sequential ionization, $Hg^{0} \rightarrow Hg^{+} \rightarrow Hg^{++}$.

The magnitude of $Hg^{++}/Hg^{+}$ observed in these experiments is in good agreement with the results of Pawlik et al[4] for those ions emerging near the axis of the ion thruster. Relationship of the response of the two probes is given in Appendix A, which follows. From the treatment there it is shown that the ion TOF probe results should be compared to Pawlik's on-axis data.

The $Hg^{++}/Hg^{+}$ ratio has been shown to depend in an approximately linear fashion on $n_e$, the electron density in the discharge. This, like the threshold data, is strong evidence for the sequential ionization process for $Hg^{++}$ production. [Any two-step process, for example $Hg^{0} \rightarrow Hg^{0*}$ (metastable) $\rightarrow Hg^{++}$, should also possess a linear dependence on $n_e$. However, the magnitude of the cross section for $0^*$ to $2^+$ transitions makes this reaction an unlikely source of $Hg^{++}$].

The ++/+ ratio has been examined and found to be invariant with respect to variations in the ion deceleration fields following acceleration and with respect to variations in ion divergence angle relative to the thrust beam axis. Both aspects of this behavior are expected.

The ++/+ ratio has been found to be parametrically described by $kI_b(V_A - 22)$ where $I_b$ is ion beam current and $(V_A - 22)$ is anode voltage minus 22 volts and is approximately $[(V_A - V_{keeper}) - V_{threshold}]$ where $V_{threshold}$ is the appearance potential for ionization of $Hg^{+}$ to $Hg^{++}$. This relationship has been observed to hold for high propellant utilization conditions. However, in a "spoiled" discharge with poor propellant utilization conditions, marked variations of the ++/+ ratio away from this stated parametric dependence have been observed. This behavior has also

been examined as anode current was varied. Within a range of anode current from approximately seven to approximately fourteen times ion beam current, the ++/+ ratio remained fixed.

The apparent decoupling between anode current and discharge plasma density (variations of $I_b$ through variations in propellant flow and with fixed anode voltage and current, and constancy of $I_b$ with varying anode current) raises interesting questions. Kaufman and Cohen[9] state that primary electron density is linearly dependent on anode current. However, to compare results from these experiments to Kaufman and Cohen may require a fixed expenditure in ev/ion as other parameters in the discharge are varied. For those experiments in which $I_b$ was varied through neutral injection rate, the ev/ion cost remained above the 300 to 400 ev/ion figure but did vary inversely with $I_b$. Similarly, for fixed $I_b$ and varying anode current, the ev/ion cost remained above 300 to 400 ev/ion point, but varied directly with anode current.

A final aspect of these experiments is the possibility they reveal of using the doubly charged ion abundance as a probe of plasma discharge behavior. Admittedly, the ++/+ ratio is an involved result of the ion history as the particle moves through the discharge, and does not provide a point-by-point diagnosis of that discharge. However, the ++/+ ratios are easily and quickly obtained and do provide an indication of discharge behavior without the (possibly disruptive) insertion of material probes into that discharge.

## APPENDIX A

## ESTIMATE OF PROBE SENSITIVITY FUNCTION

In comparing the results of $Hg^{++}/Hg^{+}$ ratios obtained here to those obtained by Pawlik et al,[4] attention must be given to acceptance characteristics of the two probes. The Pawlik probe accepts a well-collimated ion beam and, hence, "looks" at only a small portion of the ion engine accel surface at a given probe position. Results of Pawlik, then, describe the ++/+ ratio as a function of radial exit position on the accel grid, and a diminution of this ratio as the probe viewing point moves from the axis of the thruster to the outer edge of the discharge region has been observed.[4]

The transverse field ion TOF probe has a larger acceptance range on the ion entrance angle, and, qualitatively speaking, "looks" at the entire "active" face of the accel grid. However, certain portions of the accel grid are viewed with more sensitivity than others, because of geometrical factors in the probe inlet channel and sensing Faraday cup. The probe entrance aperture is a 1- by 3-cm rectangular opening followed by a series of deflecting plates extending about 4.5 cm into the probe housing. The accel grid-to-probe entrance distance is $\sim$1 meter and the probe entrance-to-Faraday cup separation is $\sim$60 cm. Ions originating on the axis of the ion engine and passing through the entrance aperture will illuminate an area on the Faraday cup of $\simeq\frac{160}{100}$ (1 x 3) cm.

This area is totally contained within the limits of the Faraday cup, and the inlet solid angle acceptance is at maximum value so the "sensitivity" to ion detection is evaluated at 1.00. Within a narrow range of area over the face of the accel grid this sensitivity remains at 1.00. Outside of this area, ions have a diminished solid angle of acceptance through the probe inlet. Also, the illuminated area at the plane of the Faraday cup may not be completely contained within the sensing area of the cup. When these two geometrical factors are evaluated, a sensitivity function for the entire active area of the accel grid is determined. This function is given in Figure 16.

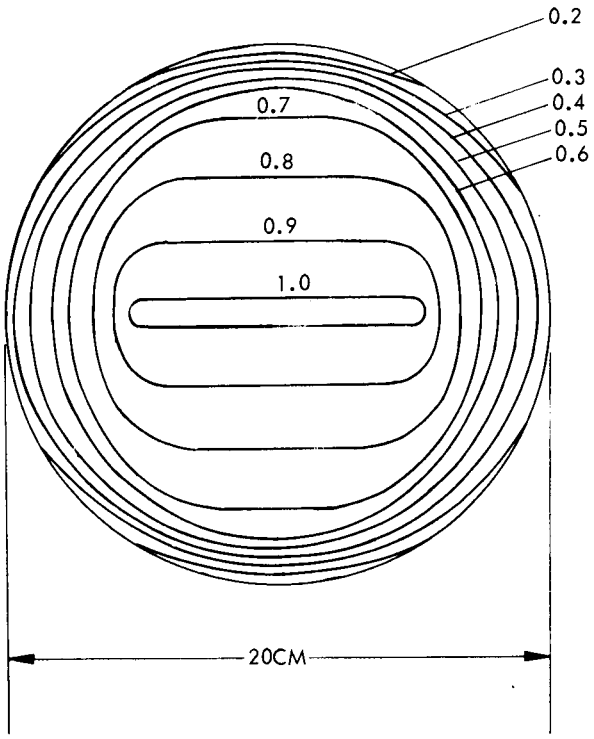


Figure 16. A Ray-Tracing Estimate of the Sensitivity Function of the Time-of-Flight Probe to Various Regions of the Ion Engine Grid Normalized to Center

The variation in sensitivity for ion acceptance over the face of the accel grid will not result in variations in the measured ++/+ ratio if the ++/+ production ratio in the discharge is invariant over this same area. However, if the ++/+ ratio should diminish in moving away from the engine axis, and Pawlik's results indicate such a diminution, then corrections of the experimental data from the TOF probe must be made. Such corrections involve the calculated sensitivity function and the measured dependence of $J_+$ over the accel grid. Expressed in integral form:

$$\left(\frac{I_{++}}{I_+}\right)_{true} = \int_{beam\ area} \left(\frac{J_{++}}{J_+}\right)\left(\frac{J_+}{I_+}\right) dA \qquad (A\text{-}1)$$

$$\left(\frac{I_{++}}{I_+}\right)_{measured} = \frac{\int_{beam\ area}\left(\frac{J_{++}}{J_+}\right)\left(\frac{J_+}{I_+}\right) S\ dA}{\int_{beam\ area}\left(\frac{J_+}{I_+}\right) S\ dA} \qquad (A\text{-}2)$$

where $\left(\frac{J_{++}}{J_+}\right)$, $\left(\frac{J_+}{I_+}\right)$, and S (the sensitivity function), are all functions of position over the area of the beam. In the absence of the measured behavior of $\left(\frac{J_+}{I_+}\right)$ over the beam area, the correction from Equation (A-2) to Equation (A-1) cannot be made. It should be noted, however, that S is generally large where $\left(\frac{J_+}{I_+}\right)$ has its maximum values for this bombardment discharge, and, hence, the measured ++/+ ratios are accurate representations of the overall beam specie currents and of the ++/+ ratios on and near the axis of the ion engine. In making comparison with Pawlik's results, then, the TOF probe will be compared to the on-axis results of that probe (Figure 11, Reference 4).

## REFERENCES


1. N. L. Milder, "Comparative Measurements of Singly and Doubly Ionized Mercury Produced by Electron Bombardment Ion Engine," NASA TN D-1219, Lewis Research Center, Cleveland, Ohio, July 1962.

2. R. F. Kemp, J. M. Sellen, and E. V. Pawlik, "Beam Neutralization Tests of a Flight Model Electron Bombardment Engine," ARS Paper 2663-62, Presented at the 17th Annual Meeting and Space Flight Exposition, Los Angeles, Calif., November 1962. Also NASA TN D-1733, July 1963.

3. T. D. Masek, "Plasma Properties and Performance of Mercury Ion Thrusters," Technical Report 32-1483, Jet Propulsion Laboratory, Pasadena, California, June 15, 1970.

4. E. V. Pawlik, et al, "Ion Thruster Performance Calibration," AIAA Paper 72-475, Presented at the 9th AIAA Electric Propulsion Conference, Bethesda, Maryland, April 17-19, 1972.

5. Frank T. Wu, "Ionization Processes in Mercury Discharges," TM 33-596, Jet Propulsion Laboratory, Pasadena, California, March 1, 1973.

6. T. D. Masek, "Plasma Characteristics of the Electron Bombardment Ion Engine," Jet Propulsion Laboratory, Pasadena, California, TR-32-1271 (1968).

7. Paul J. Wilbur, private communication.

8. H. R. Kaufman, "Ion-Thruster Propellant Utilization," Colorado State University, Ph.D. Thesis (1971).

9. H. R. Kaufman, and Allan J. Cohen, "Maximum Propellant Utilization in an Electron-Bombardment Thruster," Proceedings of the Symposium on Ion Sources and Formation of Ion Beams, Brookhaven National Laboratory, Upton, New York, October 19-21, 1971.

10. J. M. Sellen, "Spacecraft-Space Plasma Equilibria for Passive and Active Spacecraft," AIAA Paper 67-702, Presented at the AIAA Electric Propulsion and Plasmadynamics Conference, Colorado Springs, Colorado, September 11-13, 1967.

11. S. C. Brown, ed., Basic Data of Plasma Physics, Cambridge, Mass., MIT Press, p. 155, 1966.

12. E. V. Pawlik, private communication.